nature ecology & evolution

ARTICLES

PUBLISHED: 17 FEBRUARY 2017 | VOLUME: 1 | ARTICLE NUMBER: 0082

Transitions between phases of genomic differentiation during stick-insect speciation

Rüdiger Riesch[1†*], Moritz Muschick[2†], Dorothea Lindtke[3†], Romain Villoutreix[3†], Aaron A. Comeault[4], Timothy E. Farkas[5], Kay Lucek[3], Elizabeth Hellen[3], Víctor Soria-Carrasco[3], Stuart R. Dennis[6], Clarissa F. de Carvalho[3], Rebecca J. Safran[7], Cristina P. Sandoval[8], Jeff Feder[9], Regine Gries[10], Bernard J. Crespi[10], Gerhard Gries[10], Zach Gompert[11†*] and Patrik Nosil[3*]

Speciation can involve a transition from a few genetic loci that are resistant to gene flow to genome-wide differentiation. However, only limited data exist concerning this transition and the factors promoting it. Here, we study phases of speciation using data from >100 populations of 11 species of *Timema* stick insects. Consistent with early phases of genic speciation, adaptive colour-pattern loci reside in localized genetic regions of accentuated differentiation between populations experiencing gene flow. Transitions to genome-wide differentiation are also observed with gene flow, in association with differentiation in polygenic chemical traits affecting mate choice. Thus, intermediate phases of speciation are associated with genome-wide differentiation and mate choice, but not growth of a few genomic islands. We also find a gap in genomic differentiation between sympatric taxa that still exchange genes and those that do not, highlighting the association between differentiation and complete reproductive isolation. Our results suggest that substantial progress towards speciation may involve the alignment of multi-faceted aspects of differentiation.

Speciation involves genetic differentiation[1–3]. In the absence of gene flow, genome-wide differentiation can readily build by selection and drift. Differentiation with gene flow is potentially more complex, as the homogenizing effects of gene flow must be countered[1–3]. The genic model of speciation proposes that specific genetic regions subject to strong divergent natural or sexual selection become resistant to gene flow (that is, exhibit 'reproductive isolation') before others[4,5]. This model thus predicts localized, and potentially few, regions of accentuated differentiation or 'genomic islands' at the initiation of speciation[1,6]. It also predicts that genes subject to divergent selection reside in regions of accentuated differentiation. Consistent with such patterns, colour-pattern differences between subspecies of crows and races of butterflies map to a few localized peaks of genetic differentiation[7–9].

As speciation progresses, additional genetic regions differentiate and the effects of reproductive isolation become more genome-wide[1,3–5], either because genomic islands grow, background differentiation lifts or a combination of these processes. Differentiation need not be uniform as, for example, regions experiencing particularly strong selection or reduced recombination still exhibit the greatest differentiation[1,3,10]. Nonetheless, widespread differentiation is predicted in this 'genomic' phase of speciation. Evidence for divergent selection promoting this process (rather than genome-wide drift) is bolstered if: (1) gene flow is still appreciable; (2) genome-wide differentiation is correlated with environmental differences or traits under divergent selection (that is, genome-wide 'isolation-by-adaptation')[11,12]; and (3) genome-wide responses to selection are confirmed with experiments[13–15]. Genome-wide differences have been documented in herring[16], mosquitoes[17] and apple-maggot flies[10,14], and genome-wide isolation-by-adaptation has been reported in many organisms[11,12]. Notably, theory predicts genomic differentiation can be promoted by polygenic adaptation[3], epistasis[18], the coupling of differentiation across loci (as in hybrid zone theory)[19] and mate choice[20,21].

Genic and genomic phases of speciation represent extremes on a quantitative spectrum where differentiation transitions from localized to genome-wide (Fig. 1). This view is consistent with many models of speciation and with the biological species concept[2,3,22–24]. Indeed, reproductive isolation eventually becomes a property of the entire genome[25]. Although this spectrum provides a conceptual and theoretical framework for analysing speciation[1,3–5,19,26], empirical understanding of it is limited. This is because replicated genomic studies across the spectrum are still restricted to a few systems, such as cichlid fish[27], stickleback[28], flycatchers[29] and *Heliconius* butterflies[30] (reviewed by ref. [1]). Work on these systems suggests that localized differentiation is promoted by divergent selection and reduced recombination, but that genome-wide differentiation can evolve early in speciation[1,27–30]. However, uncertainties remain

[1]School of Biological Sciences, Royal Holloway, University of London, Egham, Surrey TW20 0EX, UK. [2]Aquatic Ecology & Evolution, Institute of Ecology and Evolution, University of Bern, CH-3012, Bern, Switzerland. [3]Department of Animal and Plant Sciences, University of Sheffield, Sheffield, South Yorkshire S10 2TN, UK. [4]Department of Biology, University of North Carolina, Chapel Hill, North Carolina 27599, USA. [5]Department of Ecology and Evolutionary Biology, University of Connecticut, Storrs, Connecticut 06369, USA. [6]Department of Aquatic Ecology, Eawag Swiss Federal Institute of Aquatic Science and Technology, Überlandstrasse 133, 8600 Dübendorf, Zurich, Switzerland. [7]Department of Ecology and Evolutionary Biology, University of Colorado, Boulder, Colorado 80309, USA. [8]Department of Ecology, Evolution, and Marine Biology, University of California, Santa Barbara, California 93106, USA. [9]Department of Biology, Notre Dame University, South Bend, Indiana 11111, USA. [10]Department of Biological Sciences, Simon Fraser University, Burnaby, British Columbia V5A 1S6, Canada. [11]Department of Biology, Utah State University, Logan, Utah 84322, USA. [†]These authors contributed equally to this work. *e-mail: p.nosil@sheffield.ac.uk; rudiger.riesch@rhul.ac.uk; zach.gompert@usu.edu

about underlying speciation processes and the role of genomic islands[23,26,31]. Additional studies of phases of genomic differentiation are required, especially if generalities are to be established.

Here, we study genomic differentiation in *Timema* stick insects, testing the predictions described above (Fig. 1). We report localized differentiation associated with colour-pattern loci. We find a transition to genome-wide differentiation despite gene flow, associated with mate choice. Indeed, we observe appreciable genome-wide differentiation in sympatry (for example, mean Wright's fixation index (F_{ST}) ≈ 0.10, ranging up to 0.27). However, we find little evidence for the growth of genomic islands and report that maximal differentiation is associated with a lack of measurable gene flow. The context-dependent nature of the results renders arguments about the 'importance' of the above factors subjective; different factors affect different aspects of differentiation (Fig. 1).

Our data also quantify the 'speciation continuum'. A fairly uniform speciation process should leave an observable and interconnected continuum of populations varying in differentiation[32], a pattern now reported in plant and animal taxa[1]. For example, pea aphid host races vary quantitatively in levels of genetic differentiation[33] and natural hybridization between butterflies declines gradually with genetic distance[34]. However, theory predicts that speciation can also be a less-uniform process with variable dynamics across time or space, due to changes in gene flow, sudden coupling of differentiation across loci[3], waiting time for mutations[18], nonlinear accumulation of genetic incompatibilities[18,35] and rare founder events[25]. If such dynamics cause sudden increases, decreases or halts in the accumulation of differentiation, then 'gaps' in the speciation continuum may be observed. With sufficient sampling, such gaps can be recognized by a paucity of intermediate forms (that is, bimodal distributions). The frequency and causes of gaps remain open questions, which we help address here.

Study system, background and approach

Timema are wingless, plant-feeding insects found in southwestern North America[36]. Previous work in *Timema cristinae* has shown that divergent selection between conspecific populations on different host plants (ecotypes hereafter) promotes adaptive differentiation, most markedly in colour-pattern traits conferring crypsis against visual predators[37,38]. Ecotypes also exhibit mate choice and partial sexual isolation, but this is not based on colour pattern[37,38] (Figs 1 and 2). Several studies have shown substantial gene flow between *T. cristinae* ecotypes[13,39]. Specifically, there are some 50 N_em (number of effective migrants per generation) in populations found in the same locality and ~5–10 N_em in populations separated by 1–10 km[13,39]. As in most other systems[1,2], the dynamics of speciation from its onset to end are unresolved.

We use data from thousands of individuals from >100 host-plant-associated populations of 11 sexual *Timema* species to tackle this issue. Our study includes genomic data suitable for population-level analyses and genome-wide association (GWA) mapping, such as genotyping-by-sequencing (GBS) data and low-coverage whole-genome re-sequencing data from >1,000 individuals (see Methods; Supplementary Fig. 4). There are four aims: (1) to test whether genetic regions harbouring colour-pattern loci exhibit accentuated genetic differentiation between *T. cristinae* ecotypes; (2) to test whether differentiation in traits affecting mate choice is associated with sexual isolation and genome-wide differentiation in *T. cristinae*; (3) to quantify genomic patterns of differentiation in multiple *Timema* ecotypes and species; and (4) to examine the time course to complete reproductive isolation.

In past work, genetic differentiation between *T. cristinae* ecotypes was quantified at the fine scale of single-nucleotide polymorphisms (SNPs)[13]. This approach revealed numerous modest-size regions (that is, thousands of base pairs) of accentuated and parallel differentiation that were spread across linkage groups (LG). A between-generation transplant-and-sequence experiment showed that these regions were statistically enriched for regions that were probably affected by divergent selection between hosts. Thus, previous work already suggests that divergent selection promotes fine-scale differentiation across many genetic regions during the early phases of speciation. Here, our interest is in the transition to larger-scale differentiation. Thus, rather than analysing SNPs, we estimated differentiation metrics (for example, F_{ST}) in 20-kilobase (kb) windows and used a hidden Markov model (HMM)[40] approach to assign windows to larger, contiguous regions of accentuated or background differentiation. This means that our results concern large genomic blocks (or in other cases, mean genome-wide differentiation). Fine-scale differentiation exists for individual SNPs, or clusters of them, even in cases where blocks of accentuated differentiation are not detected.

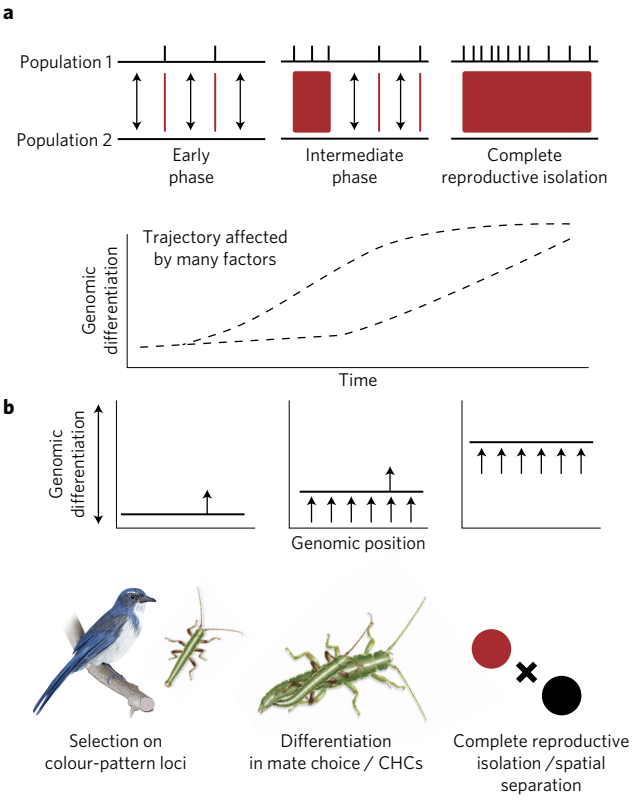

Figure 1 | Conceptual overview and summary of genomic differentiation in *Timema*. a, Phases of speciation and genomic differentiation. Genetic differentiation (red boxes) spreads to involve more of the genome as speciation progresses. Double-headed arrows represent gene flow between populations. Ticks above the horizontal line for population 1 represent genetic regions affected by divergent selection. The trajectory of increase in genomic differentiation can be affected by many factors, such as the genetic architecture of traits under selection, strength of selection, recombination rate variation, migration rate between populations and so on[1]. The top dotted line in the graph represents conditions where genome-wide differentiation evolves early during speciation. The bottom dotted line represents cases where genomic differentiation may be restricted to a few regions ('islands') for a substantial portion of the speciation process. **b**, Summary of patterns of genomic differentiation in *Timema*. Divergent selection on colour-pattern loci is associated with localized differentiation, increased genome-wide differentiation is associated with cuticular hydrocarbons (CHCs) and the most pronounced levels of differentiation are associated with very low gene flow (that is, due to complete reproductive isolation or strong spatial separation). Because genome-wide differentiation appears common in *Timema*, its trajectory may mirror the top dotted line in **a**. Panel **a** adapted from ref. [4], Wiley.

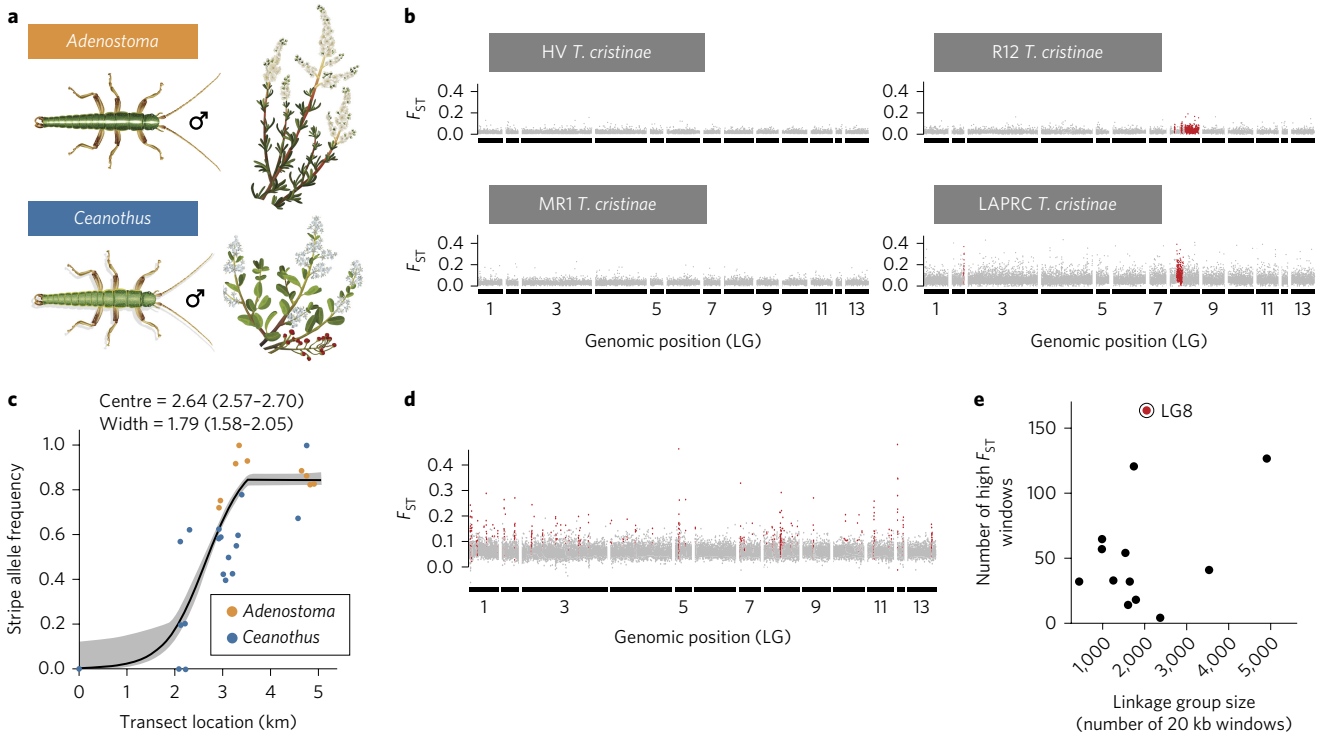

Figure 2 | Localized genetic differentiation (F_{ST}) in *T. cristinae*. **a**, Illustrations of *Adenostoma* and *Ceanothus* ecotypes of *T. cristinae* and their host plants. **b**, HMM analysis of heterogeneous genetic differentiation showing regions of accentuated F_{ST} (in red) relative to the genome-wide background (in grey). SNPs associated with colour-pattern map to LG8 and are found in regions of accentuated differentiation more than expected by chance. **c**, A steep cline in allele frequency at the colour-pattern locus, inferred from morph frequencies (grey shaded area is ±95% credible intervals). **d**, HMM analysis of the differentiation between experimental populations on different hosts from the within-generation transplant experiment, showing regions of accentuated F_{ST} in red. The *y* axis has been corrected for minor variation in F_{ST} at the onset of the experiment and thus represents differentiation that evolved between the onset and completion of the experiment. **e**, The number of regions of accentuated differentiation per LG as a function of LG size, in the transplant experiment (note the highest concentration for LG8).

Given subtle allele frequency differences and high gene flow between conspecific ecotypes, our whole-genome analyses of within-species variation focus on F_{ST}. Indeed, genome-wide differentiation between ecotypes studied here is sufficiently weak that Nei's measure of absolute divergence (D_{XY}) is near perfectly correlated to nucleotide diversity (π; for all conspecific ecotype pairs the correlation between D_{XY} and π is >0.99, Pearson correlation). Thus, D_{XY} within species effectively measures diversity, not differentiation. We do report patterns of D_{XY} when considering whole genomes of species pairs, because of their strong differentiation. We note that our conclusions side against speciation being associated with one or a few islands of differentiation. Thus, most criticisms of the use of F_{ST} to study speciation do not apply, because these criticisms are based on the argument that F_{ST} overestimates the importance of genomic islands for reduced gene flow[31]. Also, F_{ST} as an estimate of genome-wide, rather than localized, differentiation is not subject to these criticisms. As described below, we use analytical tools in addition to F_{ST} to bolster inferences (for example, approximate Bayesian computation, GWA mapping, model-based analyses of genetic structure and phylogenetic inference).

Results and discussion

Colour-pattern loci are associated with localized genetic differentiation. We tested whether loci affected by divergent selection exhibit accentuated differentiation between *Ceanothus* and *Adenostoma* host-plant ecotypes of *T. cristinae*. We considered a colour-pattern trait (a white dorsal stripe) that is subject to divergent natural selection between these hosts due to visual predation[41] (Fig. 2). GWA studies within a polymorphic population and genetic crosses have shown that this trait is largely controlled by one or few regions on LG8 (ref. [42]). However, differentiation of this region between ecotypes in nature is untested.

We found three lines of evidence that divergent selection on colour pattern promotes localized differentiation (Fig. 2 and Supplementary Fig. 2). First, we sampled a geographic cline that transitions from an area dominated by *Ceanothus* to one dominated by *Adenostoma*. Based on 1,598 individuals collected across 33 sites, we inferred allele frequencies from phenotype frequencies using knowledge of the genetic basis of colour pattern[42] (Supplementary Fig. 3 and Supplementary Table 10). We found a steep cline in colour-pattern allele frequencies, with some analyses showing near fixed differences at a distance of ~5 km. Genome-wide differentiation between ecotypes is weak at this distance[13] ($F_{ST} \approx 0.03$). Although this evidence is indirect, it suggests colour-pattern loci overcome gene flow more strongly than the remainder of the genome.

Second and more directly, we found that SNPs associated with colour pattern reside in regions of accentuated differentiation between ecotypes. Using published data[42] and GWA analyses, we mapped colour pattern (% dorsal body area striped) and confirmed that SNPs strongly associated with this trait were restricted to LG8. Using 160 previously published genomes[13], we estimated regions of accentuated F_{ST} between four ecotype pairs with the HMM[40] approach. We detected such regions for only two of the four pairs and they were only modestly elevated over background levels. This finding suggests that gene flow has strong homogenizing effects at the scale of the large genomic blocks analysed here. Nonetheless, SNPs associated with colour pattern coincide with HMM regions of accentuated differentiation between

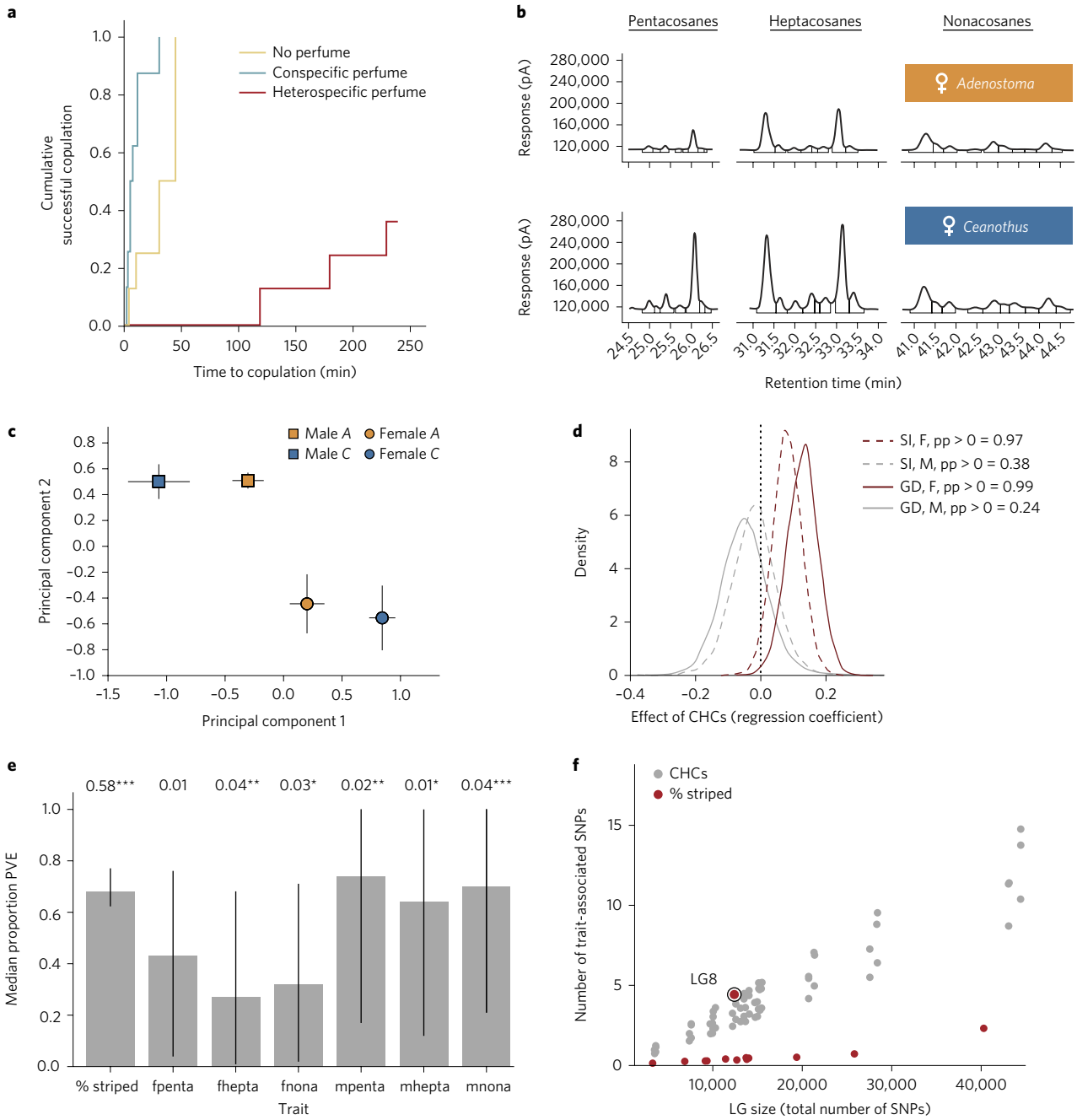

Figure 3 | CHCs and genome-wide differentiation in *T. cristinae*. **a**, Time to copulation as a function of perfuming treatment. **b**, Profiles of representative methylated cuticular hydrocarbon (CHC) profiles of females from two host-plant ecotypes (pA = picoAmpere). **c**, Differences between sexes and host ecotypes in CHCs (means ± 95% confidence intervals). *A* = *Adenostoma*, *C* = *Ceanothus*. **d**, Tests as to whether male (M, grey lines) or female (F, red lines) CHCs are associated with sexual isolation (SI) or mean genome-wide differentiation (GD), after controlling for geographic distance; pp distributions for the effect size on each variable are shown. **e**, Proportion PVE by genotype in GWA mapping. Bars show posterior medians and lines denote the 95% equal-tailed probability intervals. Shown in boxes above each bar are r^2 values from cross-validation analyses (asterisks denote significance: $^*P < 0.05$, $^{**}P < 0.01$, $^{***}P < 0.001$). % striped = per cent of body area striped, fpenta = female pentacosanes, fhepta = female heptacosanes, fnona = female nonacosanes, mpenta = male pentacosanes, mhepta = male heptacosanes, mnona = male nonacosanes. **f**, LG partitioning showing the number of trait-associated SNPs as a function of LG size.

ecotypes approximately 12-fold more often than expected by chance ($P = 0.0033$; randomization test).

Third, a within-generation transplant-and-sequence experiment using 473 new whole genomes from *T. cristinae* revealed that the highest concentration of genetic differentiation between populations transplanted to different hosts occurred on LG8 (Fig. 2). Thus, the observed number of windows assigned to the high differentiation state on LG8 was approximately two- to threefold greater than expected by chance (observed = 164, null = 63, $P < 0.001$; randomization test). Nonetheless, we did observe differentiation on other LGs. Coupled with past SNP-based analyses[13], the results suggest that divergent selection promotes differentiation of modest-sized

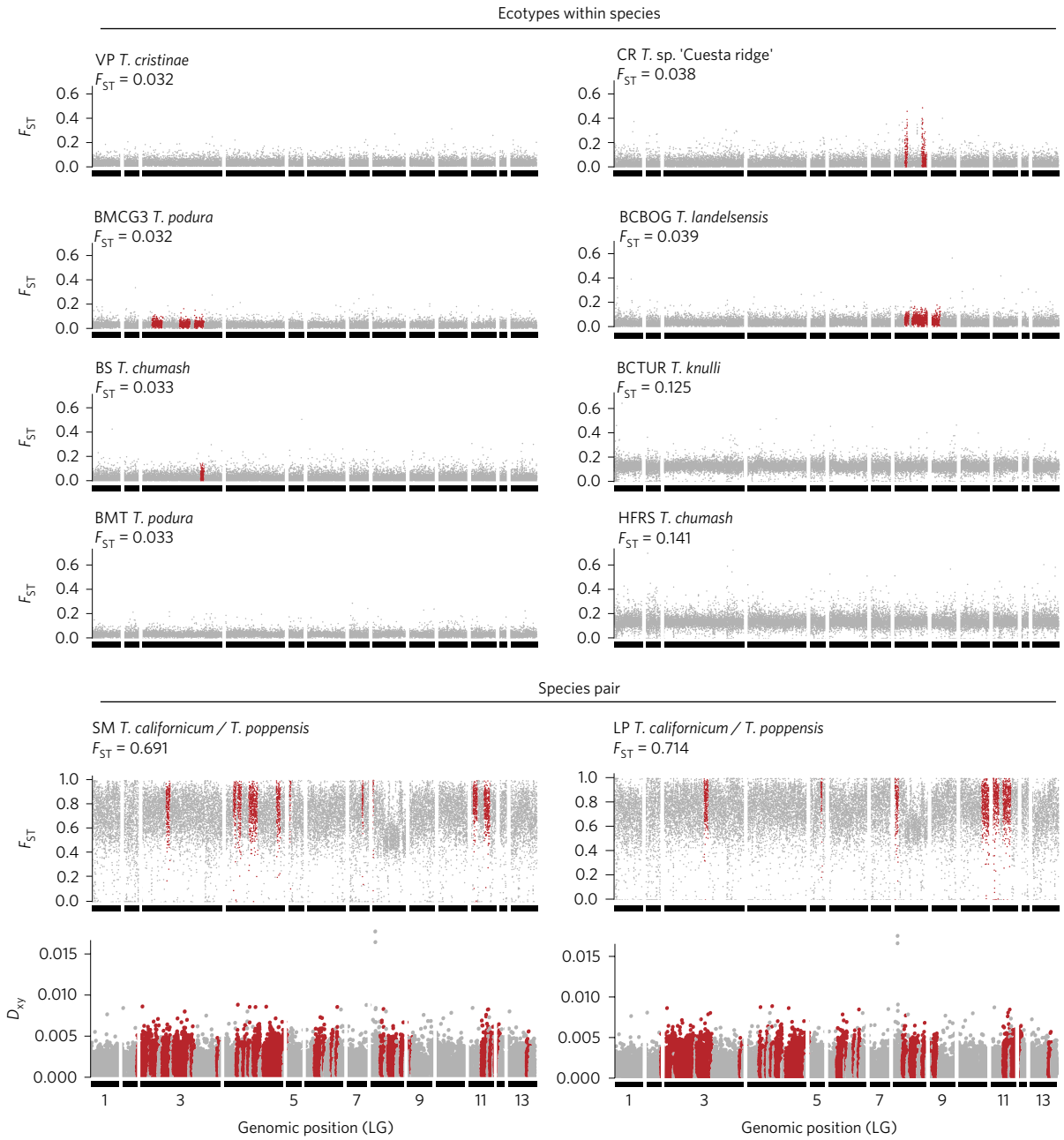

Figure 4 | Whole-genome analyses of genomic differentiation (F_{ST}) in *Timema*. HMM analysis of heterogeneous genetic differentiation, showing regions of accentuated differentiation (in red) relative to the genome-wide background (in grey). Abbreviations by the species names are locality codes and all taxon pairs are found on different host plants. Mean F_{ST} results are shown for regions of background differentiation.

regions on multiple LGs[13] and larger-scale differentiation on the LG containing colour-pattern loci.

Colour-pattern loci are not associated with genome-wide differentiation. We next tested for associations between trait differentiation and mean genome-wide F_{ST} (that is, genome-wide isolation-by-adaptation). We did so using GBS data for 21 pairwise comparisons for which data exist on sexual isolation[43]. These populations occur at the 1 to 10 km scale of restricted but non-zero gene flow. After controlling for geographic distance, we found no evidence that population differentiation in colour pattern has an effect on mean genome-wide F_{ST}; the posterior probability that the effect was >0 (pp hereafter) was <0.60, $n = 21$ (Bayesian linear mixed model, BLMM). Thus, effects of colour pattern on genetic differentiation are localized in the genome, consistent with this trait being largely controlled by a single LG and that it does not affect mate choice[44].

Cuticular hydrocarbon variation and its genetic basis. We next studied cuticular hydrocarbons (CHCs). We did so because CHC differentiation is inversely correlated with mating probability between *Timema* species[45] and CHCs affect mate choice in other insects[46]. Thus, CHCs could affect genomic differentiation. We quantified the genetic basis of CHCs and tested their association with mate choice and genomic differentiation.

We quantified three classes of CHCs and found strong sexual dimorphism (sex effect, $F_{6,334} = 56.86$, $P < 0.001$, Wilks' partial η^2 effect

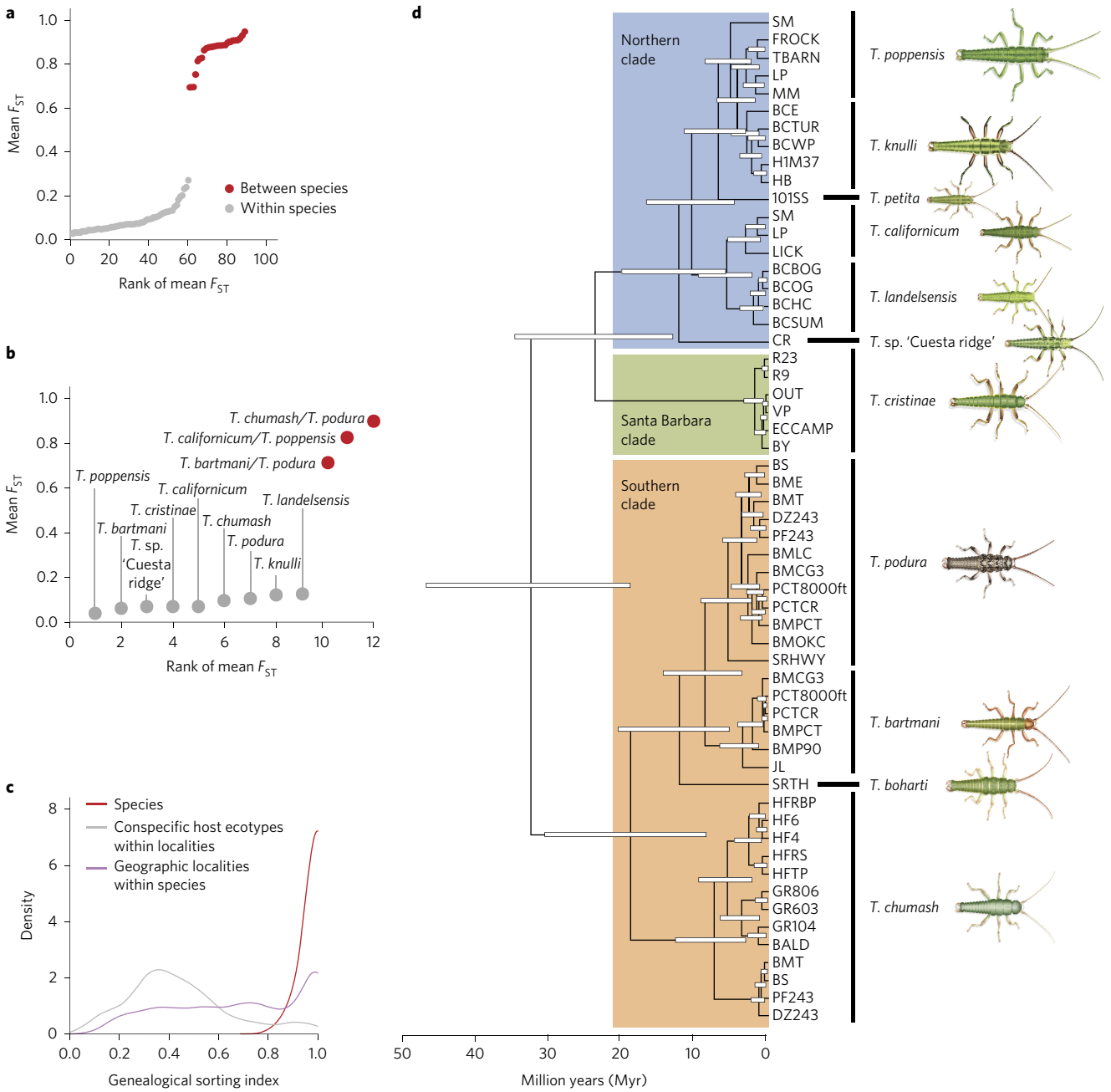

Figure 5 | A gap in genomic differentiation (mean genome-wide F_{ST}) for *Timema* taxa in sympatry. a, A gap in genome-wide F_{ST} between conspecific host-plant-associated populations and species within the same locality (that is, 'sympatry'), estimated using GBS data. **b**, The gap using mean values per species and species pairs. **c**, GSI analysis shows a paucity of intermediate values between conspecific ecotypes and species (note that species level is restricted to species sympatric with other species). **d**, Time-calibrated phylogenetic tree of the relationships between the *Timema* populations and species studied in our survey of 1,505 individuals from 11 species in 47 geographic localities (= 57 tips in the tree). Bayesian posterior probabilities were >0.97 for all nodes in the tree.

size = 50.5; host-plant effect, $F_{6,334} = 13.90$, $P < 0.001$, partial $\eta^2 = 20.0$; multivariate analysis of variance; Fig. 3). We thus quantified the genetic architecture of CHCs in males and females separately. GWA mapping supports a polygenic basis to CHCs with a modest but non-zero heritability. We observed a correlation between the number of CHC-associated SNPs per LG and LG size ($r > 0.99$, $P < 0.01$, for all six combinations of two sexes and three CHC classes, that is, 'traits'; Fig. 3). This pattern argues against major locus control, but could arise if CHCs were completely non-heritable or via heritable variation with polygenic control[47]. We distinguished these alternatives by testing whether CHC variation was partially explained by genotype, which would support non-zero heritability. Consistent with this hypothesis, we found that estimates of the median phenotypic variance explained (PVE) by genotype were ~30% in females and ~60% in males, albeit with wide credible intervals around these point estimates (Fig. 3, Supplementary Fig. 2 and Supplementary Tables 6–8). Moreover, we detected low but significant predictive power in cross-validation (that is, genomic prediction) analyses for five of six CHC traits (Supplementary Table 8). Low predictive power is expected for polygenic traits[48], but even limited predictive power strongly suggests non-zero heritability.

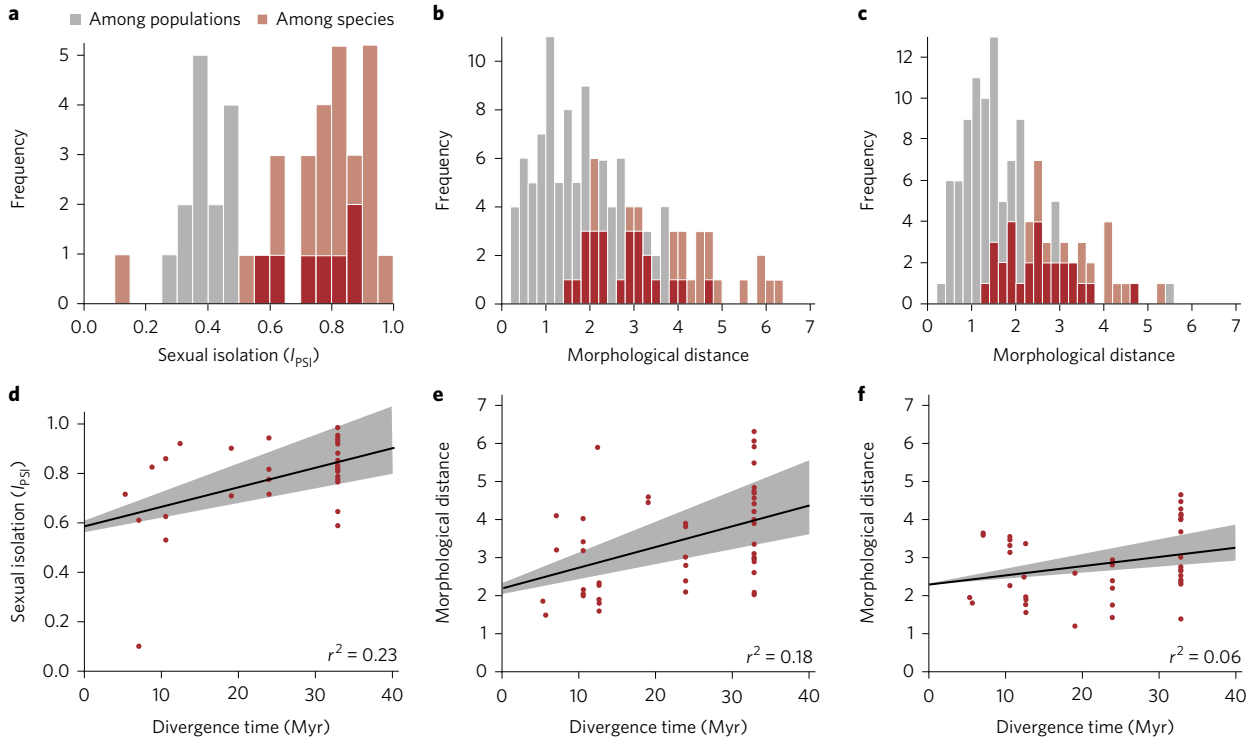

Figure 6 | Temporal dynamics of the evolution of sexual isolation and morphological differentiation. a–c, Differences within and between species in sexual isolation (**a**, measured by the I_{PSI} index) and morphological differentiation (**b**, males; **c**, females). Dark red signifies overlapping parts of the distributions shown. **d–f**, Sexual isolation (**d**) and morphological differentiation (**e**, males; **f**, females) between species against divergence time (Myr = million years; which in *Timema* is equal to millions of generations). The regression lines fitted using divergence times from the dated molecular phylogeny are shown in black; 95% confidence intervals in grey shading were obtained by fitting regression lines to the 2.5% and 97.5% quantiles of the distribution of divergence times obtained from 1,000 trees from the posterior distribution.

CHCs and mate choice. We conducted perfuming experiments and found that female CHCs causally affect mate choice within a population of *T. cristinae* and sexual isolation between a species pair (treatment effects, log rank $X^2 = 28.211$, $P < 0.001$; all *post hoc* pairwise comparisons, $P < 0.01$; Fig. 3 and Supplementary Table 9). As recently reported for *Drosophila* CHCs[46], the relation between mate choice within species and sexual isolation is not necessarily straightforward. Although we do not know for certain the extent to which female CHCs cause sexual isolation between conspecific populations (this was not tested experimentally), some effect seems probable given that the perfuming experiments show causal effects on mate choice within species and sexual isolation between species, and given that population differentiation in female CHCs in *T. cristinae* is positively correlated with degree of sexual isolation (partial coefficient controlling for geographic distance = 0.08, pp = 0.97; partial coefficient controlling for genome-wide $F_{ST} = 0.08$, pp = 0.96, $n = 21$, BLMM; Fig. 3).

In contrast, male CHCs seem unlikely to affect mate choice. This is because males choose females as mates in *Timema*[49] and population differentiation in male CHCs is not correlated with sexual isolation (partial coefficient controlling for geographic distance = −0.02, pp = 0.38; partial coefficient controlling for genome-wide $F_{ST} = -0.02$, pp = 0.38, $n = 21$, BLMM).

CHCs are associated with genome-wide differentiation. CHCs in *T. cristinae* appear polygenic. The effects of polygenic traits on genomic differentiation are difficult to predict. On the one hand, their differentiation affects many genetic regions. On the other hand, their differentiation may be difficult to achieve with gene flow, due to weak per locus selection coefficients[6]. We found that population differentiation in female CHCs was positively correlated with mean genome-wide F_{ST} after controlling for geographic distance (partial coefficient = 0.13, pp = 0.99, BLMM; Fig. 3). In contrast, differentiation in male CHCs was not (pp < 0.60). As for the analyses with colour pattern, the populations examined occur at the 1 to 10 km scale of restricted but non-zero gene flow. Thus, an association of polygenic traits with mate choice might be important for genome-wide differentiation with gene flow. However, the correlational nature of this analysis urges future work on causal associations between trait divergence, gene flow and genetic differentiation.

Estimates of heritability (that is, PVE) of female CHCs were modest but non-zero. Thus, their association with reproductive isolation and with genomic differentiation probably involves genetic factors. Nonetheless, environmentally induced effects almost certainly contribute, as for most quantitative traits[48]. Induced effects on reproductive isolation have been reported for imprinting of song in birds[50], cultural differences among killer whale ecotypes[51] and host or mate preference in insects[52]. However, if environmental effects can be reversed, this could decrease reproductive isolation. Further work on the role of genes versus induced effects in speciation is warranted. We next tested if the localized and genome-wide differentiation observed in *T. cristinae* was representative of that in the genus broadly and of potentially more advanced phases of differentiation.

Genomics of the speciation continuum in *Timema*. We collected whole-genome re-sequence data from 379 *Timema* across 10 taxon pairs. Eight pairs were conspecific ecotypes (within six species) and the other two were species pairs within two localities. Half of the conspecific ecotype pairs examined exhibited a few HMM regions of accentuated differentiation, which were usually only modestly elevated above background levels (Supplementary Tables 4 and 5).

The other half lacked such regions. We found some variation in genome-wide F_{ST} among comparisons, but this appeared unrelated to the presence or number of regions of accentuated differentiation (Fig. 4). Approximate Bayesian computation and island-equilibrium analyses support gene flow between all conspecific ecotype pairs (Supplementary Fig. 1).

These results imply that the early to moderate phases of *Timema* speciation involve more than just growth of a few islands of differentiation. Rather, localized genetic changes may be associated with only restricted progress towards speciation unless they align with mate choice, other forms of reproductive isolation or factors promoting genome-wide differentiation (for example, geographic separation). Indeed, the species pair (*T. poppensis* and *T. californicum*) showed both strong genome-wide differentiation and multiple regions of accentuated differentiation (Fig. 4 and Supplementary Tables 4 and 5; D_{XY}, locality Summit (SM): background = 0.00116, accentuated = 0.00203, 23 accentuated regions with a mean size of 374.8 20-kb windows, equalling 33.8% of the 20-kb windows; locality Loma Prieta (LP): background = 0.00115, accentuated = 0.00199, 20 accentuated regions with a mean size of 445.9 20-kb windows, equalling 35.0% of the 20-kb windows). We suspect the alignment of multi-faceted aspects of differentiation could be important for speciation in many systems where reproductive isolation evolves in a polygenic fashion.

Mean genome-wide differentiation between sympatric ecotypes. Genome-wide differentiation appears common in *Timema*; therefore, we quantified the extent of it when the potential for gene flow is high (that is, sympatry). We estimated genome-wide F_{ST} based on GBS data obtained from sampling across the geographic and host ranges of 11 *Timema* species at 47 localities (n = 1,505 specimens) (Fig. 5 and Supplementary Table 1). This yielded 89 within-locality comparisons ('sympatry'). Sixty of these were between conspecific host ecotypes and 29 were between three different pairs of species. This sampling covers most variation in geographic range and host use in these species and includes all of the known sympatric sexual species pairs in the genus[36].

We observed a continuum of differentiation among sympatric ecotypes, with genome-wide F_{ST} ranging from 0.03 to 0.27 (mean = 0.09) (Fig. 5). The upper end of differentiation is thus appreciable, but never exceeded 0.30. Model-based analyses in ENTROPY[53] support gene flow and admixture between sympatric ecotypes (Supplementary Fig. 1 and Supplementary Tables 2 and 3). The geographic potential for gene flow was similar among ecotypes (that is, all comparisons are sympatric). Thus, variation in genome-wide F_{ST} probably reflects, in part, the strength of reproductive isolation. However, other factors such as demographic variability, time in geographic contact and subtle variation in arrangement of host plants most probably contribute.

A gap in genomic differentiation restricted to sympatry. In contrast to ecotypes, mean F_{ST} between sympatric species was high at all localities (range 0.70 to 0.95, mean = 0.86). We thus observed a lack of sympatric forms with 'intermediate' F_{ST} values between 0.30 and 0.70, representing a gap in the speciation continuum. To study this gap while accounting for non-independence of pairwise F_{ST} estimates, we estimated a phylogeny-based genealogical sorting index (GSI)[54]. Largely consistent with the F_{ST}-based results, we found strong bimodality in the distribution of GSI values for sympatric taxa, with a paucity of values intermediate between those characteristic of ecotypes and species (Fig. 5).

In contrast to sympatry, we found that conspecific populations in different localities (that is, outside of sympatry) exhibit a wide range of differentiation, including levels intermediate between sympatric ecotypes and species (range of mean F_{ST} = 0.04 to 0.88, mean = 0.43, n = 579 pairwise comparisons; Fig. 5 for GSI). Specifically, such populations showed positive associations between mean F_{ST} and geographic distance (slope within all species > 0.30, all pp > 0.98; Bayesian Regression).

Analyses in ENTROPY[53] revealed little or no admixture between sympatric species, consistent with strong or complete reproductive isolation (Supplementary Fig. 1 and Supplementary Tables 2 and 3). The documented gap between sympatric ecotypes and species probably reflects intraspecific gene flow (that is, incomplete reproductive isolation) that prevents maximal differentiation from forming or being maintained in sympatry. In principle, the gap could be due to rapid sympatric speciation. However, this is difficult theoretically[2,18] and it does not match biogeographic patterns in *Timema*, where range overlap between taxonomically recognized species is slight or absent[36]. Our results suggest that gene flow can contribute to evolutionary gaps. Specifically, gene flow can make intermediate phases of speciation difficult to observe because these phases occur rapidly (for example, in reverse), rarely or restricted in space. In such cases, gaps are 'apparent' rather than real, and extensive sampling is required to observe the intermediate states.

The evolution of complete reproductive isolation. We have shown that maximal genomic differentiation in *Timema* is associated with complete reproductive isolation[13]. We thus studied the evolution of complete reproductive isolation. We did so in the context of allopatric or completely reproductively isolated species. Dynamics with gene flow could be different than described below.

We quantified sexual isolation between *Timema* species from published data[45]. This revealed some overlap within and between species, but greater sexual isolation on average between species (Fig. 6). To study temporal dynamics of sexual isolation, we used divergence times between species extracted from a Bayesian phylogenetic time-tree inferred using the GBS data from our genus-wide survey and dated with fossil-based secondary calibrations (Supplementary Tables 11–14). This approach revealed that sexual isolation accumulates gradually through time until it approximates completion (that is, ~1; Fig. 6). Strong sexual isolation requires tens of millions of years (*Timema* are univoltine, with one generation per year). Morphological differentiation in colour and other traits probably reduces the time to complete reproductive isolation, by causing ecological isolation[37,38]. However, morphological differentiation estimated here (n = 978) also evolves gradually between species such that complete reproductive isolation by sexual isolation plus ecological isolation probably requires substantial time (Fig. 6 and Supplementary Tables 11 and 12). The long time frames required for strong reproductive isolation via the reproductive barriers measured here suggest that speciation in *Timema* involves other barriers, such as genetic incompatibilities. Moreover, completion of reproductive isolation could involve long periods of geographic isolation. Future work on the most advanced stages of *Timema* speciation is warranted.

Conclusions

We have shown that the transition from localized to genome-wide differentiation can be observed despite gene flow and may be aided by mate choice. Overall, our results accord well with models of parapatric speciation[18], but do not support a strong role for the growth of a few islands of differentiation, at least for early to intermediate phases of speciation. Details of the evolution of strong reproductive isolation in *Timema* remain unclear, but the existence of a wide range of differentiation outside of sympatry facilitates future studies of many phases of speciation and the role of coupling of differentiation across loci[3]. The myriad of effects reported here, and the modesty of some of them, indicate that future work on the relative importance of each (rather than merely its presence) is justified. Despite the need for further work, our results show that integrative studies do allow even complex speciation processes to begin to be understood.

Methods

Summary. We combined linkage mapping, phenotypic and experimental data, GWA mapping, GBS data and whole-genome re-sequence data from 1,012 *Timema* individuals (160 genomes re-analysed from ref. [13] and 852 new to this study, 473 of which originated from the transplant experiment and 379 from natural populations of eight species). Supplementary Table 15 provides an overview of the data used in this study that were previously published, the data that are new and the relation between the two.

For whole genomes, coverage is as follows: natural taxon pairs, mean coverage is ~1.1× per individual and ~22.0× per population; transplant experiment ~1.4× per individual and ~139.4× per experimental block. Coverage for GBS data was higher, as outlined below. In all cases, we infer genotypes probabilistically and thus account for genotype uncertainty (details below). Such approaches are increasingly common in large-scale analyses in model systems, are not reliant on 'calling' genotypes with certainty and are suitable for robust inferences using low-coverage data across many individuals[55,56].

Due to the size and complexity of our integrative dataset, we provide the core methods below in sufficient detail to evaluate our study. Further details concerning, for example, read counts, sample populations and parameter settings, are contained in the Supplementary Information.

Morph frequency cline. We sampled *T. cristinae* at 33 collection sites in 1996 and again in 2001. We collected a total of 1,598 individuals, and scored each as green-unstriped, green-striped, green-intermediate or melanistic (by C.S. in 1996 and by C.S. and P.N. in 2001). We first considered just the green-striped and green-unstriped morphs, because these can be scored unambiguously and because the stripe is recessive, such that green-striped morphs are homozygous for the stripe allele and can be used to estimate the frequency of the major-effect stripe allele[42]. We obtained estimates of the stripe allele frequency for each site by pooling data across years (as results were similar across years) and by assuming that all striped individuals were homozygous for the stripe allele and Hardy–Weinberg equilibrium. We fit a six-parameter cline model for the stripe allele frequencies[57] using the R 3.2.3 package hzar 0.2–5 (ref. [58]). We inferred cline parameters in a Bayesian framework using Markov chain Monte Carlo (two million iterations with a one-million iteration burn-in). To assess the robustness of our results, we repeated this analysis including individuals scored as intermediate, assuming they were green-striped morphs and then assuming they were green-unstriped morphs. We observed a qualitatively similar conclusion of a steep cline in all analyses, although quantitative details varied among the analyses (Supplementary Fig. 3).

Whole-genome analyses of published *T. cristinae* genomes. We conducted novel analyses of larger-scale heterogeneity in genetic differentiation between the *Adenostoma* and *Ceanothus* ecotypes of *T. cristinae*. The analyses based on 20-kb windows thus differ from previous work that analysed fine-scale differentiation of SNPs for these same ecotypes. We used a HMM to identify contiguous genomic regions with accentuated differentiation between each of four previously studied *T. cristinae* ecotype pairs (Hidden Valley *Adenostoma* (HVA) × Hidden Valley *Ceanothus* (HVC), Mark Recapture 1 *Adenostoma* (MR1A) × Mark Recapture 1 *Ceanothus* (MR1C), Refugio 12 *Adenostoma* (R12A) × Refugio 12 *Ceanothus* (R12C), and Laurel *Adenostoma* (LA) × Paradise *Ceanothus* (PRC)). These data were described in ref. [13] and include 160 whole-genome sequences. We first calculated F_{ST} for non-overlapping 20-kb windows as $F_{ST} = (\pi_t - \pi_w)/\pi_t$, where π_w is the mean nucleotide diversity within ecotypes and π_t is the nucleotide diversity for both ecotypes combined. Note that we calculated our estimate as a ratio of means across sites (rather than a mean of ratios) as suggested by ref. [59]. We then fit an HMM with two discrete states for the logit-transformed F_{ST} estimates for each ecotype pair, assuming logit F_{ST} was normally distributed. We defined a background differentiation state with a mean and standard deviation that matched the empirical mean and standard deviation and an accentuated differentiation state with the same standard deviation but a mean set to the 90th empirical quantile of the F_{ST} distribution. We estimated the transition matrix between states using the Baum–Welch algorithm and we used the Viterbi algorithm to predict the most probable sequence of hidden states from the data and estimated parameters[60]. We used the R 3.0.2 package HiddenMarkov 1.7.0 to fit these models[61,62] but modified the code to use fixed values for state means and standard deviations (this allowed us to explicitly test islands of accentuated differentiation). We defined HMM regions of accentuated differentiation as the contiguous set of 20-kb windows showing a high differentiation state within an LG (but potentially spanning multiple scaffolds).

Co-localization of stripe-associated SNPs and HMM regions of accentuated differentiation. We applied this analysis to the four pairs of *Ceanothus* and *Adenostoma* ecotypes of *T. cristinae*[13], which are known to be subject to divergent selection on colour pattern. We used a permutation test to ask whether stripe-associated SNPs from our GWA mapping (described in 'GBS and GWA mapping', below) occurred in high HMM regions across the four ecotype pairs more often than expected by chance. However, as only two pairs had high HMM regions (on LG8 for R12A × R12C and LGs 1 and 8 for LA × PRC), this is really a test of whether stripe-associated SNPs were in high HMM regions more than expected by chance for these two pairs. We focused on SNPs with posterior inclusion probabilities for stripe that were greater than 0.1. Such SNPs occurred in seven unique 20-kb windows. Across the four pairs, the windows with stripe-associated SNPs were also high HMM windows 20% of the time. Randomization of high HMM regions (10,000 randomizations, with the size of HMM regions kept constant) indicated that high HMM regions and trait-associated SNP regions overlapped more than expected by chance (null expectation = 1.7%, $P = 0.0033$). We obtained similar results when considering stripe-associated SNPs with posterior inclusions probabilities greater than 0.05 (17 unique 20-kb windows, observed overlap = 14%, null expectation = 1.7%, $P = 0.0003$).

Whole-genome transplant-and-sequence experiment. As the procedures for implementing this experiment have been previously described[63], we provide only a brief overview. We collected and transplanted 500 *T. cristinae* from an area dominated by *Adenostoma* (population Far Hill *Adenostoma* (FHA)) onto either an individual of their native host plant (*Adenostoma*) or the alternative host plant (*Ceanothus*). As previously described[63], there is little to no dispersal in such experimental settings, including the experiment analysed here. After eight days, we recaptured surviving insects. Following previously published protocols[13], we then extracted DNA, prepared individually barcoded sequencing libraries and conducted whole-genome re-sequencing of the 500 insects. We successfully obtained data from 473 individuals, which we analysed further. We aligned the paired-end sequences to the *T. cristinae* reference genome using the BWA–MEM algorithm in BWA 0.7.5a-r405 (ref. [64]). We then identified variant nucleotides using the UnifiedGenotyper in GATK 3.1 (ref. [65]) (ignoring scaffolds not assigned to LGs) and estimated genotypes using an empirical Bayesian approach, as in past work[63].

We quantified genetic differentiation between survivors from the two host-plant treatments by calculating F_{ST} for 20-kb windows, as described in the previous section. We likewise calculated F_{ST} at the onset of the experiment, verifying that genetic differentiation at the start was low to non-existent. We then fit the same HMM described in the previous section to delineate accentuated regions of genetic differentiation between survivors on *Adenostoma* versus *Ceanothus*, controlling for minor variation in genetic differentiation at the onset of the experiment by subtracting initial F_{ST} from F_{ST} between the survivors. We conducted a randomization test (1,000 permutations of HMM window states) to determine whether HMM windows assigned to the high differentiation state occurred on LG8 more than expected by chance.

Quantifying dorsal colour pattern (% body area striped). We recorded digital images of 873 adult *T. cristinae* (539 males and 334 females) using previously described methods[42]; 592 of these images (395 males and 197 females) originated from a previous study that considered a single population on *Adenostoma* (FHA, that is, one ecotype in one locality) and that used the images to quantify and map colour pattern (% striped)[42]. Here, we estimated % striped for the full set of photos, including eight populations on *Ceanothus* and ten on *Adenostoma*. These data were collected to facilitate tests on the effect of colour pattern on genomic differentiation among populations, but GWA was restricted to individuals from the large sample in FHA. We estimated % striped by dividing the area of the stripe by the total dorsal body area, each estimated using the 'polygon selection tool' in ImageJ, as previously described[42].

CHC variation. We sampled 20 populations of *T. cristinae* (8 on *Ceanothus* and 12 on *Adenostoma*) for a total of 915 insects (559 males and 356 females; Supplementary Table 6). As above, a subset of these originated from the FHA population reported in ref. [42], but ecotype differences in CHCs or the genetic basis of CHCs were not examined in this previous study. We cold-euthanized live insects and subsequently submerged them in separate vials with 1 ml of high-performance liquid chromatography-grade hexane for 10 min to extract CHCs from their body surface. Using a 6890 Hewlett Packard gas chromatograph, we quantified 26 different mono- and di-methylated CHCs for each insect: eight pentacosanes, eight heptacosanes and ten nonacosanes. As is standard practice in studies of CHCs[45], we analysed their proportional rather than absolute abundance; this allowed us to reduce experimental error and to remove individual differences originating from variation in insect body size[66,67]. We calculated CHC proportions by dividing the amount of each CHC in a given sample by the sum of all quantified CHCs in that sample. We then transformed these CHC proportions using log-contrasts[66,68] to remove the non-independence among analysed variables. We calculated log-contrasts by dividing the value for each CHC by the value of the CHC 5-methylheptacosane (5Me27) and then taking the $\log_{10}$ of these new variables, resulting in 25 log-contrast transformed values for every insect. We found all 25 CHC-measurements to be highly repeatable and the results obtained by dividing by values of other CHCs to be similar (Supplementary Information). To further reduce data dimensionality and to account for multicollinearity, we conducted a principal component analysis (on a covariance matrix with promax rotation) and retained principal component axes with an eigenvalue larger than the mean eigenvalue as variables in a multivariate analysis of variance to test for effects due to 'sex', 'host plant' and the interaction of 'sex and host plant' (12 populations on *Adenostoma* and 8 on *Ceanothus*).

GBS and GWA mapping. We obtained genotypes for mapping with 592 *T. cristinae* from the FHA population using the sequencing reads from these insects previously published[42]. This previous study mapped colour pattern (% striped) but not the other traits considered here. We used the software GEMMA 0.94 (ref. [48]) to implement Bayesian sparse linear mixed models (BSLMMs) that estimate the genetic architecture of traits while also considering relatedness of individuals within the sample. BSLMMs in GEMMA provide estimates of the proportion of phenotypic variation that can be explained by the combined effects of polygenic (infinitesimal effect) and measurable (modest to larger) effect SNPs. We thus estimated three hyper-parameters for each trait: (1) the total proportion of PVE by genotype (that is, estimated heritability); (2) the proportion of the genetic PVE that is due to the effects of measurable-effect SNPs; and (3) the number of measurable-effect SNPs. GEMMA also provides posterior inclusion probabilities (also called γ parameter) for each SNP that reflect the fraction of Markov chain Monte Carlo iterations of the BSLMM for which a given SNP had a measurable effect on phenotypic variation (that is, this reflects the weight of evidence that individual SNPs are associated with the trait of interest).

We estimated the above-mentioned hyper-parameters and posterior inclusion probability values for the following traits: (1) % striped; (2) the proportion of methylated pentacosanes, heptacosanes and nonacosanes in females; and (3) the proportion of methylated pentacosanes, heptacosanes, and nonacosanes in males. We tested for an association between the number of trait-associated SNPs per LG and the LG size; a strong positive correlation is predicted for polygenic traits[47]. Finally, we performed cross-validation (that is, genomic prediction) analyses to test the predictive power of our GWA mapping[69].

Perfuming trials with no-choice copulation experiments. We conducted 24 no-choice copulation trials (eight trials each with 'conspecific native population perfume', 'heterospecific perfume' or 'no perfume') between one male and one female *T. cristinae* from FHA (males choose mates in *Timema*)[49]. Each individual perfume consisted of CHCs that we extracted from six cold-euthanized females and gently transferred to the live female in each trial. No-choice copulation trials were based on previously published protocols[70]. For each trial, we kept one male and one female *T. cristinae* in a 10 cm Petri dish for 4 h and we scored the latency to copulate (that is, minutes until copulation)[49]. We conducted perfuming trials during the same time (8:45 am to 12:45 pm) on different days, but always ran the same number of 'conspecific' and 'heterospecific' perfuming trials simultaneously. We analysed the latency to copulate by means of a Kaplan–Meyer analysis in IBM SPSS Statistics 21.

Tests for effects of colour pattern and CHCs on sexual isolation and genome-wide F_{ST}. These analyses focused on seven *T. cristinae* populations previously studied for sexual isolation, for which we also obtained data on colour pattern, CHCs and F_{ST} ($n=21$ pairwise comparisons). We estimated the strength of sexual isolation between populations by calculating the index of pairwise sexual isolation (I_{PSI} index; theoretical range -1 to $+1$, where -1 = complete disassortative mating, 0 = random mating and $+1$ = complete sexual isolation; all our empirical values were positive)[71]. Specifically, we calculated pairwise I_{PSI} scores based on mating propensity derived from no-choice mating trials published in a previous study[43]. To estimate CHC differences between populations, we first conducted principal component analyses separate for each sex (on a covariance matrix with promax rotation) on CHC data from these seven populations. We retained principal component axes with an eigenvalue larger than the mean eigenvalue to calculate sex-specific pairwise Euclidian CHC distances between populations. We estimated population differentiation in colour pattern using data on morph frequencies (green-striped versus green-unstriped) collected between 2000 and 2008 (population, % striped morph, sample size: Poppy *Ceanothus* (PC), 18%, 505; HVA, 85%, 1,383; Mattress *Adenostoma* (MA), 82%, 310; LA, 86%, 654; Outlook *Adenostoma* (OUTA), 49%, 631; PRC, 1%, 1,261; Open Grass *Ceanothus* (OGC), 74%, 168).

To obtain F_{ST} estimates, we combined new GBS data for 325 samples from 19 *T. cristinae* populations with 17 randomly chosen samples (10 males and 7 females) from the FHA mapping population, resulting in sequences from 342 individuals spanning 20 populations (5–20 individuals per population, mean = 17) for population genetic analyses of genetic differentiation. We mapped reads to the reference genome with BOWTIE2 2.2.3 (ref. [72]) and called variants with SAMTOOLS 0.1.19 mpileup and BCFTOOLS 0.1.19 (ref. [73]) using the full prior and requiring the probability of the data being homozygous for the reference allele to be less than 0.01. We estimated genome-wide Hudson's F_{ST} (refs [74,75]) for all 190 population pairs using allele frequencies estimated from genotype probabilities obtained as in ref. [13]. We retained 613,261 bi-allelic SNPs with a mean coverage depth per SNP per individual of ~5× (per SNP average ranging from 2.2 to 28.7; per individual average ranging from 1.0 to 10.3).

We estimated genome-wide Hudson's F_{ST} (refs [74,75]) for all 190 population pairs as $F_{ST} = 1 - H_w/H_b$, where H_w is the mean number of differences among sequences from the same population and H_b is the mean number of differences among sequences from different populations, averaged over loci. We calculated H_w and H_b for each locus from population allele frequencies estimated using genotype probabilities obtained with SAMTOOLS and BCFTOOLS[76], as in ref. [13]. For each population pair, we excluded loci with a minor allele frequency less than 0.05 or where less than 50% of individuals were covered.

We used these data for subsequent tests of how colour pattern and CHCs affect sexual isolation and mean F_{ST}. As reported in the main text, we fit BLMMs to test for effects of population differentiation in these traits on sexual isolation and mean F_{ST} while accounting for geographic distances among populations and the correlated error structure of pairwise distance data[53,77]. We did this using either sexual isolation or logit-transformed mean F_{ST} as the response variable (for sexual isolation we also conducted analyses replacing geographic distance with mean F_{ST} as the covariate being accounted for). Linear models included population-specific random effects, geographic distances and one of the three following variables as predictors of sexual isolation or F_{ST}: (1) colour-pattern distances (% difference between populations in striped individuals); (2) male CHC distances; or (3) female CHC distances. We centred and standardized covariates before analyses. We specified uninformative priors for the regression coefficients (normal priors with mean (μ) = 0, variance (σ^2) = 1,000) and for the gamma (shape parameters: $\alpha = 1$, $\beta = 0.01$) hyper-priors on the precision (inverse variance) for the random effects[53]. We ran three independent Markov chain Monte Carlo chains, each with 5,000 iterations, a 1,000 iteration burn-in and a thinning interval of five for each model. We then calculated the posterior probability that the standardized partial regression coefficient for colour pattern, male CHC or female CHC distance was greater than zero (this is valid as the effect of having pairwise observations is accounted for by the population random effects)[53,77].

Whole-genome re-sequencing of ten population pairs spanning eight species. Following previously published protocols[13], we sequenced and further analysed an additional 379 *Timema* genomes (these are a subset of the 1,505 described below for which we obtained GBS data). We aligned the paired-end sequences to the *T. cristinae* reference genome using the BWA-MEM algorithm in BWA 0.7.5a-r405 and identified SNPs using the UnifiedGenotyper in GATK. We used an expectation-maximization algorithm to obtain maximum-likelihood-allele-frequency estimates for each of the 20 populations (10 'parapatric' population pairs) for each of 5.07 million identified SNPs. We then used these maximum-likelihood-allele-frequencies to calculate sequence-based estimates of F_{ST} between each of the ten co-occurring taxon pairs, as described under 'Whole-genome analyses of published T. cristinae genomes', for ecotypes of *T. cristinae*. In addition, we determined D_{XY} (ref. [78]) for each 20-kb window for the two heterospecific population pairs (LP and SM). We used approximate Bayesian computation to estimate migration rates between these 'parapatric' taxa based on a non-equilibrium Wright–Fisher model with gene flow and also provide estimates under an island-equilibrium model[79]. We used the HMM[40] approach employed in *T. cristinae* to assign each of the 20-kb windows into groups of background or accentuated (that is, 'high') levels of differentiation. Finally, we quantified minor allele frequencies for HMM regions of accentuated differentiation (for the taxon pairs where such regions were detected) and compared them to minor allele frequencies for the genomic background. We did so for the previously published ecotype pairs[13], and the ten pairs with new whole-genome data (Supplementary Table 5).

GBS and stages of speciation. We sampled 47 widely distributed geographic localities across California for *Timema*, with the over-arching goal of sampling the greatest possible diversity of hosts, localities and sexual *Timema* species. In total, we collected 1,545 individuals of 12 *Timema* species (one sample was from an asexual species) from 13 host-plant genera. The dataset includes all the Californian sexual species of *Timema* (the others are found outside California). We extracted DNA and prepared libraries for GBS sequencing of all these individuals, as in previous work[39].

We aligned reads to the *T. cristinae* reference genome[13] using BOWTIE2 2.1.0 (ref. [72]). Quality control filtering resulted in a dataset of 1,505 individuals from 11 species that we used for all downstream analyses. Variants were called using SAMTOOLS mpileup and BCFTOOLS using the full prior, requiring the probability of the data to be less than 0.5 under the null hypothesis that all samples were homozygous for the reference allele to call a variant. We ignored insertion and deletion polymorphisms. For each population and variant, we inferred maximum-likelihood allele frequencies from the genotype likelihoods by means of the iterative soft expectation-maximization algorithm described in ref. [76] and measured genome-wide genetic differentiation between pairs of populations using the Hudson's F_{ST} (ref. [75]).

For conspecific populations found in different geographic localities we used a Bayesian hierarchical regression model to quantify the association between log geographic distance and logit F_{ST}. Slope and intercept terms were modelled hierarchically and allowed to vary by species. Non-informative priors were placed on the overall (across species) intercept and slope coefficients (normal ($\mu = 0$, precision (τ) = 1×10^{-6}) for means and gamma ($\alpha = 0.01$, $\beta = 0.01$) for all precision terms). Parameters were inferred using Markov chain Monte Carlo via the rjags interface with R. We ran three chains, each with a 20,000 iteration burn-in, 50,000 sampling iterations and a thinning interval of 10.

We estimated genetic structure and potential admixture using a hierarchical Bayesian model that jointly estimates genotypes and admixture proportions as implemented in the programme ENTROPY 1.2b (ref. [53]). This model is similar

to the popular STRUCTURE algorithm[80] but accounts for sequencing errors and genotype uncertainties inherent to next-generation sequencing methods in a way comparable to other approaches[81]. We estimated parameters for a model with $K=2$ population clusters for every pair of populations found at the same geographic locality but belonging to different species and $K=$ number-of-host-plants clusters for conspecific populations found at the same locality. Moreover, we used the deviance information criterion to evaluate if the models fitted better than $K=1$.

Maximum-likelihood phylogenetic inference and GSI. We inferred 1,000 maximum-likelihood bootstrap trees using the rapid heuristic algorithm implemented in RAxML 8.2.9 (refs [82,83]). We used a curated dataset of 19,556 single-nucleotide variants for 1,505 individuals, which we partitioned by LG. We calculated the GSI using the R package genealogicalSorting 0.92 (ref. [54]). GSI is a statistic that measures the degree of exclusive ancestry of groups of individuals in a tree. It ranges from zero when all the nodes of the tree are required to unite the group, to one when a group is genealogically exclusive (that is, individuals are united by the minimum possible number of nodes). For each bootstrap tree, we calculated GSI values for the 166 groups with at least two individuals delimited by species (11), species and locality (56), and species, locality and host (98). We plotted the joint distribution of GSI values from all bootstrap trees for sympatric species (5), geographic localities within species (37) and conspecific host ecotypes within localities (90) (Fig. 5c). Bootstrap trees and tables with GSI values are deposited in Dryad.

Estimation of sexual isolation and morphological differentiation within and betweeen species. We estimated sexual isolation between species by calculating the I_{PSI} index on previously published mating trial data within and between species[45]. We excluded the data from *T. boharti* due to uncertain species identification, but including them does not alter our conclusion. To measure morphological differentiation within and among species, we measured morphological traits of 978 adult individuals from different *Timema* species (Supplementary Tables 11 and 12). We captured specimens by sweep netting their host plants in localities that broadly overlap with those used in our genetic survey. We photographed specimens with a digital Canon EOS 70D camera equipped with a macro lens (Canon EF 100 mm f/2.8 L Macro IS USM) and two external flashes (Yongnuo YN560-II speedlights). We took the images with the camera set on manual, an aperture of f/14, a shutter speed of 1/250 s and flashes adjusted to 1/4 power in S2 mode in an output angle corresponding to 24 mm focal length on full frame (~84° diagonal). To avoid strong shadows and create an even, soft lighting, we diffused both flashes with LumiQuest SoftBox LTp softboxes, following the manufacturer's instructions. With these flash adjustments, we were able to standardize the light, reducing external luminosity interference. In addition to *Timema* specimens, the pictures included a ruler and a standard colour chip (Colorgauge Micro, Image Science Associates LLC). We photographed each insect at least twice, in positions that varied perpendicularly to capture the body colour without traces of gleam or shade. We linearized and corrected each picture for the white balance, adjusting the temperature and the tint based on the values obtained from the colour chip neutral grey colour (target #10), using Adobe Photoshop Lightroom 5.7 software (Adobe Systems Software). Only minor corrections were necessary, as the measurements did not vary appreciably among pictures. We adjusted pictures for the temperature to 5,950 and for the tint to +2, and exported them as TIFF files.

From the standardized images, we collected phenotypic measurements using the software ImageJ 1.4.8 (ref. [84]). We extracted the following size measurements: (1) body length (from the tip of the head to the base of the abdomen, not including external genitalia); (2) body width (the widest point of the second thoracic segment); and (3) head width (the distance between the eyes). We scaled the pictures using the ruler as reference, thus being able to convert all linear measurements from units of pixels into centimetres. To quantify variation in colour, we recorded mean RGB (red, green, blue) values using the polygon section tool and colour histogram plugin in ImageJ. We took the colour measurements on the lateral and dorsal margin of the second thoracic and fourth abdominal segments. We obtained the mean between the two measurements done in the lateral margin and between the two in the dorsal part. We then converted these raw RGB values to variables representing two colour channels and one luminance channel, as previously suggested[85]. We calculated a red-green colour channel using the relationship $(R-G)/(R+G)$, a green-blue colour channel as $(G-B)/(G+B)$ and a luminance (that is, brightness) channel as $(R+G+B)$. Although this method of measuring colour does not account for how colour is sensed by a potential receiver (for example, conspecific or predator), it does represent an unbiased quantification of colour that is useful in a comparative context.

We thus describe morphology based on size (that is, body length, body width, head width) and on colour channels, with values for lateral red-green, lateral green-blue, lateral luminance, dorsal red-green, dorsal green-blue and dorsal luminance. Following trait measurements, we performed a principal component analysis using all measured traits, extracting the scaled score of the first four axes for each individual. We conducted separate principal component analyses for each sex, given notable sexual dimorphism in the morphology. The first four axes account for 87 and 83% of the variation in males and females, respectively (Supplementary Table 12). We then estimated morphological distances using pairwise Euclidean distance values between different species and among populations within species, following ref. [86].

Phylogenetics and molecular dating. On account of the absence of *Timema* fossils and the poor fossil record of stick insects, we used secondary calibrations derived from a time-calibrated tree of insects (Supplementary Tables 13 and 14). To infer such a tree, we retrieved from GenBank sequences of nine molecular markers (four mitochondrial genes and five nuclear genes) for 41 genera belonging to 13 orders, placing particular emphasis on ensuring a good representation of stick insects and including the three main clades of *Timema*: Northern, Southern and Santa Barbara. For divergence time estimation, we chose six calibrations for phylogenetically well-supported groups based on robust fossil data (Supplementary Information; Supplementary Table 13). We carried out Bayesian phylogenetic inference with BEAST 2.1.3[87,88], which allows co-inference of tree topology and divergence times using a relaxed molecular clock and incorporating uncertainty in calibrations as priors in the form of statistical distributions. Subsequently, we used the divergence time posterior distributions for the root of *Timema* (split between the Northern and Santa Barbara clades, and the Southern clade) and the split between the Northern clade and the Santa Barbara clade for calibrating the tree of *Timema* populations based on GBS data (Supplementary Table 14). We inferred this tree using BEAST with the same curated dataset of 19,556 single-nucleotide variants used for the inference of maximum-likelihood bootstrap trees, but pooled by species and locality (for a total of 57 populations). We partitioned by LG and incorporated secondary calibrations as priors in the form of gamma distributions. Details concerning GenBank sequences, multiple alignments and phylogenetic trees are deposited in Dryad Digital Repository.

Data availability. The genetic data reported in this paper have been deposited in the National Center for Biotechnology Information (NCBI) Short Read Archive under the following BioProject Accession Numbers: PRJNA356725 (whole genomes of natural populations), PRJNA356801 (whole genomes of transplant experiments), PRJNA356911 (GBS for updating reference genome linkage mapping), PRJNA356405 (GBS for stages of speciation) and PRJNA356885 (GBS for tests on the effect of colour pattern and CHC on genome-wide differentiation). The genome draft 0.3 is available on the Nosil Lab of Evolutionary Biology website (http://nosil-lab.group.shef.ac.uk/?page_id=25) and has been deposited as an NCBI Whole Genome Shotgun project (accession number MSSY03000000). Phenotypic data, processed genetic data and code used for analysis have been archived in Dryad Digital Repository at http://dx.doi.org/10.5061/dryad.nq67q.

Received 28 May 2016; accepted 12 January 2017; published 17 February 2017

References

1. Seehausen, O. *et al.* Genomics and the origin of species. *Nat. Rev. Genet.* **15,** 176–192 (2014).
2. Coyne, J. A. & Orr, H. A. *Speciation* 1st edn (Sinauer Associates, 2004).
3. Flaxman, S., Walchoder, A., Feder, J. L. & Nosil, P. Theoretical models of the influence of genomic architecture on speciation. *Mol. Ecol.* **23,** 4074–4088 (2014).
4. Wu, C. The genic view of the process of speciation. *J. Evol. Biol.* **14,** 851–865 (2001).
5. Mallet, J. A species definition for the modern synthesis. *Trends Ecol. Evol.* **10,** 294–299 (1995).
6. Feder, J. L., Egan, S. P. & Nosil, P. The genomics of speciation-with-gene-flow. *Trends Genet.* **28,** 342–350 (2012).
7. Poelstra, J. W. *et al.* The genomic landscape underlying phenotypic integrity in the face of gene flow in crows. *Science* **344,** 1410–1414 (2014).
8. Nadeau, N. J. *et al.* Population genomics of parallel hybrid zones in the mimetic butterflies, *H. melpomene* and *H. erato*. *Genome Res.* **24,** 1316–1333 (2014).
9. Nadeau, N. J. *et al.* Genomic islands of divergence in hybridizing *Heliconius* butterflies identified by large-scale targeted sequencing. *Phil. Trans. R. Soc. B* **367,** 343–353 (2012).
10. Michel, A. P. *et al.* Widespread genomic divergence during sympatric speciation. *Proc. Natl Acad. Sci. USA* **107,** 9724–9729 (2010).
11. Nosil, P., Egan, S. P. & Funk, D. J. Heterogeneous genomic differentiation between walking-stick ecotypes: "isolation by adaptation" and multiple roles for divergent selection. *Evolution* **62,** 316–336 (2008).
12. Shafer, A. B. A. & Wolf, J. B. W. Widespread evidence for incipient ecological speciation: a meta-analysis of isolation-by-ecology. *Ecol. Lett.* **16,** 940–950 (2013).
13. Soria-Carrasco, V. *et al.* Stick insect genomes reveal natural selection's role in parallel speciation. *Science* **344,** 738–742 (2014).
14. Egan, S. P. *et al.* Experimental evidence of genome-wide impact of ecological selection during early stages of speciation-with-gene-flow. *Ecol. Lett.* **18,** 817–825 (2015).

15. Burke, M. K. How does adaptation sweep through the genome? Insights from long-term selection experiments. *Proc. R. Soc. B* **279,** 5029–5038 (2012).
16. Lamichhaney, S. *et al.* Population-scale sequencing reveals genetic differentiation due to local adaptation in Atlantic herring. *Proc. Natl Acad. Sci. USA* **109,** 19345–19350 (2012).
17. Lawniczak, M. K. N. *et al.* Widespread divergence between incipient *Anopheles gambiae* species revealed by whole genome sequences. *Science* **330,** 512–514 (2010).
18. Gavrilets, S. *Fitness Landscapes and the Origin of Species* Vol. 41 (Princeton Univ. Press, 2004).
19. Barton, N. H. Multilocus clines. *Evolution* **37,** 454–471 (1983).
20. Kirkpatrick, M. & Ravigné, V. Speciation by natural and sexual selection: models and experiments. *Am. Nat.* **159,** S22–S35 (2002).
21. Jiggins, C. D. & Mallet, J. Bimodal hybrid zones and speciation. *Trends Ecol. Evol.* **15,** 250–255 (2000).
22. Nosil, P. *Ecological Speciation* (Oxford Univ. Press, 2012).
23. Turner, T. L. & Hahn, M. W. Genomic islands of speciation or genomic islands and speciation? *Mol. Ecol.* **19,** 848–850 (2010).
24. Turner, T. L., Hahn, M. W. & Nuzhdin, S. V. Genomic islands of speciation in *Anopheles gambiae*. *PLoS Biol.* **3,** 1572–1578 (2005).
25. Mayr, E. *Animal Species and Evolution* (Harvard Univ. Press, 1963).
26. Yeaman, S., Aeschbacher, S. & Burger, R. The evolution of genomic islands by increased establishment probability of linked alleles. *Mol. Ecol.* **25,** 2542–2558 (2016).
27. Brawand, D. *et al.* The genomic substrate for adaptive radiation in African cichlid fish. *Nature* **513,** 375–381 (2014).
28. Feulner, P. G. D. *et al.* Genomics of divergence along a continuum of parapatric population differentiation. *PLoS Genet.* **11,** e1004966 (2015).
29. Burri, R. *et al.* Linked selection and recombination rate variation drive the evolution of the genomic landscape of differentiation across the speciation continuum of *Ficedula* flycatchers. *Genome Res.* **25,** 1656–1665 (2015).
30. Martin, S. H. *et al.* Genome-wide evidence for speciation with gene flow in *Heliconius* butterflies *Genome Res.* **23,** 1817–1828 (2013).
31. Cruickshank, T. E. & Hahn, M. W. Reanalysis suggests that genomic islands of speciation are due to reduced diversity, not reduced gene flow. *Mol. Ecol.* **23,** 3133–3157 (2014).
32. Darwin, C. *On the Origin of Species by Means of Natural Selection, or the Preservation of Favoured Races in the Struggle for Life* (John Murray, 1859).
33. Peccoud, J., Ollivier, A., Plantegenest, M. & Simon, J. C. A continuum of genetic divergence from sympatric host races to species in the pea aphid complex. *Proc. Natl Acad. Sci. USA* **106,** 7495–7500 (2009).
34. Mallet, J., Beltran, M., Neukirchen, W. & Linares, M. Natural hybridization in heliconiine butterflies: the species boundary as a continuum. *BMC Evol. Biol.* **7,** 28 (2007).
35. Orr, H. A. The population-genetics of speciation—the evolution of hybrid incompatibilities. *Genetics* **139,** 1805–1813 (1995).
36. Law, J. H. & Crespi, B. J. The evolution of geographic parthenogenesis in *Timema* walking-sticks. *Mol. Ecol.* **11,** 1471–1489 (2002).
37. Nosil, P. Divergent host plant adaptation and reproductive isolation between ecotypes of *Timema cristinae* walking sticks. *Am. Nat.* **169,** 151–162 (2007).
38. Nosil, P. & Sandoval, C. P. Ecological niche dimensionality and the evolutionary diversification of stick insects. *PLoS ONE* **3,** e1907 (2008).
39. Nosil, P. *et al.* Genomic consequences of multiple speciation processes in a stick insect. *Proc. R. Soc. B* **279,** 5058–5065 (2012).
40. Hofer, T., Foll, M. & Excoffier, L. Evolutionary forces shaping genomic islands of population differentiation in humans. *BMC Genomics* **13,** 107 (2012).
41. Sandoval, C. P. The effects of relative geographical scales of gene flow and selection on morph frequencies in the walking-stick *Timema cristinae*. *Evolution* **48,** 1866–1879 (1994).
42. Comeault, A. A. *et al.* Selection on a genetic polymorphism counteracts ecological speciation in a stick insect. *Curr. Biol.* **25,** 1–7 (2015).
43. Nosil, P. & Hohenlohe, P. A. Dimensionality of sexual isolation during reinforcement and ecological speciation in *Timema cristinae* stick insects. *Evol. Ecol. Res.* **14,** 467–485 (2012).
44. Nosil, P. & Crespi, B. J. Does gene flow constrain adaptive divergence or vice versa? A test using ecomorphology and sexual isolation in *Timema cristinae* walking-sticks. *Evolution* **58,** 102–112 (2004).
45. Schwander, T. *et al.* Hydrocarbon divergence and reproductive isolation in *Timema* stick insects. *BMC Evol. Biol.* **13,** 151 (2013).
46. Chung, H. *et al.* A single gene affects both ecological divergence and mate choice in *Drosophila*. *Science* **343,** 1148–1151 (2014).
47. Yang, J. *et al.* Genome partitioning of genetic variation for complex traits using common SNPs. *Nat. Genet.* **43,** 519–525 (2011).
48. Zhou, X., Carbonetto, P. & Stephens, M. Polygenic modeling with Bayesian sparse linear mixed models. *PLoS Genet.* **9,** e1003264 (2013).
49. Arbuthnott, D. & Crespi, B. J. Courtship and mate discrimination within and between species of *Timema* walking-sticks. *Anim. Behav.* **78,** 53–59 (2009).
50. Grant, B. R. & Grant, P. R. Fission and fusion of Darwin's finches populations. *Phil. Trans. R. Soc. B* **363,** 2821–2829 (2008).
51. Riesch, R., Barrett-Lennard, L. G., Ellis, G. M., Ford, J. K. B. & Deecke, V. B. Cultural traditions and the evolution of reproductive isolation: ecological speciation in killer whales? *Biol. J. Linn. Soc.* **106,** 1–17 (2012).
52. Wood, T. K. & Keese, M. C. Host-plant induced assortative mating in *Enchenopa* treehoppers. *Evolution* **44,** 619–628 (1990).
53. Gompert, Z. *et al.* Admixture and the organization of genetic diversity in a butterfly species complex revealed through common and rare genetic variants. *Mol. Ecol.* **23,** 4555–4573 (2014).
54. Cummings, M. P., Neel, M. C. & Shaw, K. L. A genealogical approach to quantifying lineage divergence. *Evolution* **62,** 2411–2422 (2008).
55. Buerkle, C. A. & Gompert, Z. Population genomics based on low coverage sequencing: How low should we go? *Mol. Ecol.* **22,** 3028–3035 (2013).
56. Fumagalli, M. *et al.* Quantifying population genetic differentiation from next-generation sequencing data. *Genetics* **195,** 979–992 (2013).
57. Barton, N. H. & Gale, K. S. in *Hybrid Zones and the Evolutionary Process* (ed. Harrison, R. G.) 13–45 (Oxford Univ. Press, 1993).
58. Derryberry, E. P., Derryberry, G. E., Maley, J. M. & Brumfield, R. T. hzar: hybrid zone analysis using an R software package. *Mol. Ecol. Resour.* **14,** 652–663 (2014).
59. Weir, B. S. & Cockerham, C. C. Estimating *F*-statistics for the analysis of population structure. *Evolution* **38,** 1358–1370 (1984).
60. Baum, L. E., Petrie, T., Soules, G. & Weiss, N. A maximization technique occurring in statistical analysis of probabilistic functions of Markov chains. *Ann. Math. Stat.* **41,** 164–171 (1970).
61. Harte, D. HiddenMarkov: Hidden Markov Models. R package version 1.7-0 (Statistics Research Associates, accessed 14 April 2012); http://cran.at.r-project.org/web/packages/HiddenMarkov
62. Harte, D. HiddenMarkov: Hidden Markov Models. R package version 1.8-3 (Statistics Research Associates, accessed 13 April 2015); http://cran.at.r-project.org/web/packages/HiddenMarkov
63. Gompert, Z. *et al.* Experimental evidence for ecological selection on genome variation in the wild. *Ecol. Lett.* **17,** 369–379 (2014).
64. Li, H. & Durbin, R. Fast and accurate short read alignment with Burrows–Wheeler transform. *Bioinformatics* **25,** 1754–1760 (2009).
65. McKenna, A. *et al.* The genome analysis toolkit: a MapReduce framework for analyzing next-generation DNA sequencing data. *Genome Res.* **20,** 1297–1303 (2010).
66. Blows, M. W. & Allan, R. A. Levels of mate recognition within and between two *Drosophila* species and their hybrids. *Am. Nat.* **152,** 826–837 (1998).
67. Rundle, H. D., Chenoweth, S. F., Doughty, P. & Blows, M. W. Divergent selection and the evolution of signal traits and mating preferences. *PLoS Biol.* **3,** e368 (2005).
68. Aitchison, J. *The Statistical Analysis of Compositional Data* 12th edn (Chapman & Hall, 1986).
69. Wray, N. R., Yang, J., Goddard, M. E. & Visscher, P. M. The genetic interpretation of area under the ROC curve in genomic profiling. *PLoS Genet.* **6,** e1000864 (2010).
70. Nosil, P., Crespi, B. J. & Sandoval, C. P. Host-plant adaptation drives the parallel evolution of reproductive isolation. *Nature* **417,** 440–443 (2002).
71. Rolan-Alvarez, E. & Caballero, M. Estimating sexual selection and sexual isolation effects from mating frequencies. *Evolution* **54,** 30–36 (2000).
72. Langmead, B. & Salzberg, S. L. Fast gapped-read alignment with Bowtie 2. *Nat. Methods* **9,** 357–359 (2012).
73. Li, H., *et al.* The sequence alignment/map format and SAMtools. *Bioinformatics* **25,** 2078–2079 (2009).
74. Hudson, R. R., Slatkin, M. & Maddison, W. P. Estimation of levels of gene flow from DNA-sequence data. *Genetics* **132,** 583–589 (1992).
75. Bhatia, G., Patterson, N., Sankararaman, S. & Price, A. L. Estimating and interpreting F_{st}: the impact of rare variants. *Genome Res.* **23,** 1514–1521 (2013).
76. Li, H. A statistical framework for SNP calling, mutation discovery, association mapping and population genetical parameter estimation from sequencing data. *Bioinformatics* **27,** 2987–2993 (2011).
77. Clarke, R. T., Rothery, P. & Raybould, A. F. Confidence limits for regression relationships between distance matrices: estimating gene flow with distance. *J. Agric. Biol. Env. Stat.* **7,** 361–372 (2002).
78. Nei, M. *Molecular Evolutionary Genetics* (Columbia Univ. Press, 1987).
79. Wright, S. Isolation by distance. *Genetics* **28,** 114–138 (1943).
80. Pritchard, J. K., Stephens, M. & Donnelly, P. Inference of population structure using multilocus genotype data. *Genetics* **155,** 945–959 (2000).
81. Skotte, L., Korneliussen, T. S. & Albrechtsen, A. Estimating individual admixture proportions from next generation sequencing data. *Genetics* **195,** 693–702 (2013).
82. Stamatakis, A. RAxML version 8: a tool for phylogenetic analysis and post-analysis of large phylogenies. *Bioinformatics* **30,** 1312–1313 (2014).
83. Stamatakis, A., Hoover, P. & Rougemont, J. A rapid bootstrap algorithm for the RAxML web servers. *Syst. Biol.* **57,** 758–771 (2008).
84. Abràmoff, M. D., Magalhães, P. J. & Ram, S. J. Image processing with ImageJ. *Biophoton. Int.* **11,** 36–42 (2004).

85. Endler, J. A. A framework for analysing colour pattern geometry: adjacent colours. *Biol. J. Linn. Soc.* **107,** 233–253 (2012).
86. Beuttell, K. & Losos, J. B. Ecological morphology of Caribbean anoles. *Herpetol. Monogr.* **13,** 1–28 (1999).
87. Bouckaert, R., Alvarado-Mora, M. V. & Pinho, J. R. R. Evolutionary rates and HBV: issues of rate estimation with Bayesian molecular methods. *Antivir. Ther.* **18,** 497–503 (2013).
88. Bouckaert, R. *et al.* BEAST 2: a software platform for Bayesian evolutionary analysis. *PLoS Comput. Biol.* **10,** e1003537 (2014).

Acknowledgements

We thank R. Guillem, R. Kather, J. Stapley and T. Schwander for their advice; the Oakley-, Kuris- and Lafferty-groups at University of California Santa Barbara for their support; L. Jeanson and J. Hosegood for the phenotypic measurements and lab work; R. Marin for drawing all the figures; T. Schwander for providing the genetic crosses used for linkage mapping; the High-Throughput Genomics Group at the Wellcome Trust Centre for Human Genetics (funded by Wellcome Trust grant reference 090532/Z/09/Z and MRC Hub grant G0900747 91070) for generating the whole-genome re-sequencing data; and the National Center for Genome Sequencing (USA) for the GBS data. R.R. was supported by the Human Frontier Science Program, M.M. and K.L. were supported by the Swiss National Science Foundation and P.N. was supported by the Royal Society of London. The work was funded by grants from the European Research Council (grant NatHisGen R/129639 to P.N.) and the Natural Science and Engineering Research Council of Canada (to B.J.C. and G.G.). Computing, storage and other resources from the Division of Research Computing in the Office of Research and Graduate Studies at Utah State University, as well as access to the High Performance Computing Facilities, particularly to the Iceberg HPC cluster, from the Corporate Information and Computing Services at the University of Sheffield, are gratefully acknowledged.

Author contributions

R.R., Z.G., M.M., G.G., J.F., B.J.C. and P.N. conceived the project. R.R., R.V., D.L., M.M., A.A.C., R.G., T.E.F., C.P.S., C.F.d.C. and P.N. collected the data. R.R., D.L., M.M., R.V., Z.G. and P.N. led the data analyses, aided by V.S.-C., K.L., C.F.d.C. and S.R.D. R.R., Z.G. and P.N. wrote the initial manuscript and all authors contributed to further writing and revisions. Z.G. and V.S.-C. organized the data archiving. R.R., M.M., D.L., R.V. and Z.G. contributed equally.

Additional information

Supplementary information is available for this paper.

Reprints and permissions information is available at www.nature.com/reprints.

Correspondence and requests for materials should be addressed to R.R., Z.G. or P.N.

How to cite this article: Riesch, R. *et al.* Transitions between phases of genomic differentiation during stick-insect speciation. *Nat. Ecol. Evol.* **1,** 0082 (2017).

Competing interests

The authors declare no competing financial interests